

How grain structure evolution affects kinetics of a solid-state reaction: a case of interaction between iridium and zirconium carbide

Ya. A. Nikiforov^{a,*}, V. A. Danilovsky^b, N. I. Baklanova^a

^a*Institute of Solid State Chemistry and Mechanochemistry SB RAS, 18 Kutateladze st., 630090, Novosibirsk, Russia*

^b*Sobolev Institute of Geology and Mineralogy SB RAS, 3/1 Koptug ave., 630090, Novosibirsk, Russia*

Abstract

This work investigates the solid-state reaction between iridium and zirconium carbide, resulting in the formation of carbon and $ZrIr_3$ —an intermetallic compound of great interest for modern high-temperature materials science. We have found a transition of kinetic regimes in this reaction: from linear kinetics (when the chemical reaction is a limiting stage) at 1500 and 1550°C to ‘non-parabolic kinetics’ at 1600°C. Non-parabolic kinetics is characterized by thickness of a product layer being proportional to a power of time less than 1/2. The nature of non-parabolic kinetics was still an open question, which motivated us to develop a model of this kinetic regime. The proposed model accounts for the grain growth in the product phase and how it leads to the time dependence of the interdiffusion coefficient. We have obtained a complete analytic solution for this model and an equation that connects the grain-growth exponent and the power-law exponent of non-parabolic kinetics. The measurements of the thickness of the product layer and the average grain size of the intermetallic phase confirm the results of the theoretical solution.

Keywords: grain growth, intermetallics, iridium, kinetics, solid state reaction, zirconium carbide

1. Introduction

Recently, iridium was proposed as a principal component for slowly oxidating protective systems [1, 2]. Indeed, it has high melting point (2446°C [3]) combined with low oxidation rate, as well as low oxygen and carbon permeability [1, 4], which makes iridium an excellent candidate for these purposes. Practical application of non-alloyed iridium coatings turned to be impossible due to recrystallization of Ir during thermal cycling that produced pores within coatings

*Corresponding author

Email address: nikiforov@solid.nsc.ru (Ya. A. Nikiforov)

[2, 5], i.e. fast-diffusion pathways. This fact did not discourage researchers, and now new approaches of alloying iridium or using multilayered coatings based on combination of iridium with tantalum, hafnium, and tungsten or their carbides/borides are explored [6, 7, 8, 9, 10, 11, 12, 13]. Components of such systems interact with each other, so a successful production and application of the coatings depends on the understanding of these interactions and resulting time-evolution of the systems.

This work is an investigation of kinetics of a reaction between iridium and zirconium carbide, one of the reaction of iridium with refractory carbides. It was shown that the reaction occurs at temperatures at least as high as 1000°C according to equation: $\text{ZrC} + 3\text{Ir} \longrightarrow \text{ZrIr}_3 + \text{C}$ [14]. The kinetics of this and similar reactions, though, is still mainly not investigated. The only relevant work, known to authors, is a study of a reaction between Ir and HfC by Kwon [15]. Kwon investigates formation of $\text{HfIr}_3 + \text{C}$ layer in the reaction between Ir and HfC at temperatures 1900–2200°C and calculates interdiffusion coefficients and activation energy of interdiffusion. Additionally, recent works on reactions between silicon carbide and transition metals [16, 17, 18, 19, 20, 21] are of some interest. Similarly to the ZrC–Ir system considered here, a metal and a carbide react in those systems, with formation of intermetallic compound(s) and carbon. It was shown, that a number of complex phenomena occur in course of reaction, although not all of them should be present in the case of ZrC–Ir. For example, a formation of periodic patterns, a common feature of reactions with SiC, was not observed in the case of Ir–HfC system. Nonetheless, an awareness of possible processes and comparison between different similar systems will be useful in interpretation of data.

We use reaction couples as a method of kinetics investigation. In this method two planar surfaces of the reactants are made into contact, heat treated at a given temperature, while the reaction products form between the reactants as a layer of nearly uniform width. Rate of solid state reaction can be limited by either rate of a reaction at interface or by transport process within bulk of products [22]. Our aim is to describe kinetics of the reaction and its dependence on temperature. During the investigation we discovered a transition between different kinetic regimes. So it was crucial to analyze these regimes and reasons why reaction proceeds according to these regimes and why the transition occurs.

For reaction couples, three kinetic regimes were observed earlier in literature [23, 24, 25, 26, 27, 28, 29, 30, 31, 32, 33, 34, 35], each being a case of reaction-limited or transport-limited reaction rate. First one is the interface reaction controlled regime, with the product layer thickness being linearly proportional to time ($\ell \propto t$) at long reaction times [36]. Second regime is the diffusion controlled regime, with the product layer thickness being proportional to the square root of time ($\ell \propto \sqrt{t}$) [37, 38]. Third regime is non-parabolic, or power-law kinetics, with layer thickness being proportional to a power of time less than 0.5 ($\ell \propto t^{1/n}$ with $n > 2$). It has been observed experimentally in some systems during last two decades [27, 28, 29, 30, 31, 32, 33, 34, 35], although this type of kinetics is less common than previous two. This regime is thought to be a type of transport process limiting, but the diffusion is not uniform as in the

second (diffusion-controlled) regime. First was suggested a model of variable diffusion coefficient due to a region of enhanced diffusion near the reaction front [39]. This diffusion enhancement was ascribed to the microstructural intricacies of a reaction zone and to a high concentration of inequilibrium defects. Later, it was suggested that grain growth in the product phase is responsible for the power-law kinetics [28, 40, 41]. These works showed that it is the most plausible explanation of non-parabolic kinetics, but the problem of an accurate generalization of this model remained. This model was developed for thin one-grain-thick intermetallics layers, and the rate exponent ($1/n$) in this model depends not only on grain growth exponent, but also on relation between layer thickness and grain size. These assumptions limit the application of the model to thin layers; meanwhile, non-parabolic kinetics was observed in thick layers [32], too. Two recent works [42, 43] examined the effect of grain growth on solid-state reaction kinetics numerically and showed a good agreement with the experiment. The numerical solution showed the validity of the proposed model and made it possible to examine cases of different ratios of bulk and grain-boundary diffusion coefficients. But, as with any numerical solution, it cannot provide an explicit functional dependence. So, a question remains: is the power law really a consequence of the grain growth within the product layer and can be derived analytically within this model, or is it only an approximation to the actual kinetic law? Thus, we aim to derive an explicit analytical solution for this model of non-parabolic growth with a minimal number of approximations.

2. Theory

To analyze the kinetics of a solid-state reaction in reaction couples, we describe mathematical models of these. Consider a situation schematically illustrated in Fig. 1. Two phases— A and B —react to form a product layer: $A + B \rightarrow PL$. The reaction takes place at an interface between PL and B (reactive boundary), while the atoms of A diffuse through the product layer PL . Atoms of A cross the boundary A/PL without the formation of a new volume of the product so that no reaction occurs, while concentration at this boundary remains constant. In this model, PL does not need to be a single phase—it is only necessary that a single interdiffusion coefficient describes the diffusion through PL . Governing equations are:

$$\frac{\partial C}{\partial t} = \frac{\partial}{\partial x} \left(D \frac{\partial C}{\partial x} \right), \quad 0 \leq x \leq \ell(t) \quad (1)$$

$$C(0, t) = C_{max} \quad (2)$$

$$\frac{1}{\bar{V}_A} \frac{d\ell}{dt} = k \cdot (C - C_{eq}) = -D \left(\frac{\partial C}{\partial x} \right) \Big|_{x=\ell} \quad (3)$$

$$\ell(0) = 0 \quad (4)$$

Eq. 1 is the second Fick's law with spatial domain from interface A/PL ($x = 0$) to the reactive boundary PL/B ($x = \ell(t)$, i.e. width of PL); D is

an interdiffusion coefficient. Eq. 2 is a boundary condition on interface A/PL . Eq. 3 is a condition on the movement of boundary PL/B : the first equal sign connects it with the rate of reaction at the interface PL/B , and the second equal sign connects it with the diffusional flux of atoms A coming from the bulk of PL towards the reactive boundary. \tilde{V}_A is a volume of PL that forms when one atom A reacts with B . C_{eq} is an equilibrium concentration of A in PL that is in contact with B . Eq. 4 is an initial condition on the width of PL .

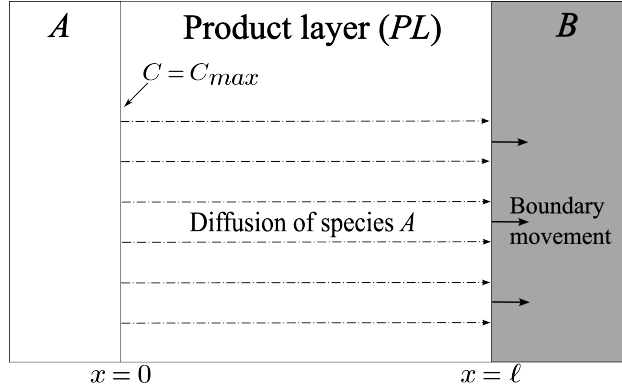


Figure 1: Scheme of the reaction couple $A + B \rightarrow PL$. Concentration of A at interface A/PL is C_{max} , meanwhile concentration at the interface PL/B may or may not be fixed depending on the particular kinetics regime.

2.1. Models of kinetics with constant interdiffusion coefficient

Commonly, an interdiffusion coefficient in Eqs. 1–4 is assumed to be constant. With this assumption, two limiting cases are possible, depending on the ratio D/k : either the interface reaction or the transport of A through PL determines the overall reaction rate. These limiting cases simplify the equation so that analytical solutions can be conveniently obtained. The derivations of these solutions can be found in [36] and [38]. Because the notation in this work differs from [36] and [38], we also give derivations in Appendix A.

For a case of interface reaction control, diffusion of A is much faster than interface reaction, and a simplification is that the concentration profile $C(x, t)$ is assumed to be linear. The solution [36] is:

$$\left\{ \begin{array}{l} \ell(t) = \frac{D}{k} \left(\sqrt{1 + 2(C_{max} - C_{eq})\tilde{V}_A \frac{k^2}{D} t} - 1 \right) \end{array} \right. \quad (5)$$

$$\left\{ \begin{array}{l} C(x, t) = C_{max} - \frac{(C_{max} - C_{eq})x}{\sqrt{1 + 2(C_{max} - C_{eq})\tilde{V}_A \frac{k^2}{D} t}} \end{array} \right. \quad (6)$$

In a case of diffusion control, the interface reaction occurs much faster than diffusion within PL . It leads to a local equilibrium on the reactive boundary so

that $C(\ell, t) = C_{eq}$, and movement of the reactive boundary is determined by the concentration gradient. The solution [38] is:

$$\begin{cases} \ell(t) = 2\gamma\sqrt{Dt} & (7) \\ C(x, t) = C_{max} - \frac{C_{max} - C_{eq}}{\text{erf}(\gamma)} \text{erf}\left(\frac{x}{2\sqrt{Dt}}\right) & (8) \\ \frac{(C_{max} - C_{eq})\tilde{V}_A}{\sqrt{\pi}} = \gamma \text{erf}(\gamma) \exp(\gamma^2) & (9) \end{cases}$$

Eqs. 5 and 7 are the kinetic laws that can be used to analyze growth of product layer in solid-state reaction.

2.2. Grain-growth accompanied kinetics

Here, we consider a situation when the interdiffusion coefficient is not constant and is affected by the grain growth in the product phase. We study this case because it was earlier proposed [28, 40, 41] that the grain growth is a reason for non-parabolic kinetics, which is described with the power law $\ell \propto t^{1/n}$ rather than with Eqs. 5 and 7. Our goal here is to obtain an analytical solution for this situation with a minimal number of assumptions. An alternative derivation, more general than here, can be found in Appendix A.3.

We treat this situation as a case of diffusion control, that is the velocity of the movement of reactive boundary is determined by a diffusion flux. Governing equations for this case are:

$$\frac{\partial C}{\partial t} = \frac{\partial}{\partial x} \left(D(x, t) \frac{\partial C}{\partial x} \right), \quad 0 \leq x \leq \ell(t) \quad (10)$$

$$C(0, t) = C_{max}, \quad C(\ell, t) = C_{eq} \quad (11)$$

$$\frac{1}{\tilde{V}_A} \frac{d\ell}{dt} = -D \left(\frac{\partial C}{\partial x} \right) \Big|_{x=\ell} \quad (12)$$

$$\ell(0) = 0 \quad (13)$$

To solve these equations, we need at first to obtain expression for the interdiffusion coefficient. Expression for interdiffusion coefficient [44] in terms of a bulk diffusion coefficient, D_B , and a grain-boundary diffusion coefficient, D_{GB} , is:

$$D = gD_{GB} + (1 - g)D_B$$

where, g is an effective volume fraction available for grain boundary diffusion and is given by the equation:

$$g = \frac{q\delta}{L} \quad (14)$$

where L is an average grain size, δ is a grain boundary width and q is a numerical factor that depends on the shape of grains.

The first approximation we use is that the bulk diffusion is negligible in comparison with grain boundary diffusion, $gD_{GB} \gg (1-g)D_B$. With that, the effective interdiffusion coefficient is:

$$D = gD_{GB} \quad (15)$$

Next, we need to account for the grain growth, which obeys the power law [45, 46]:

$$L^m - L_0^m = k(t - t_0) \quad (16)$$

where L is an average grain size at time t , L_0 is an average grain size at initial time t_0 , k is a constant of grain growth.

The second approximation is that the initial grain size is negligibly small, $L_0 \approx 0$. It simplifies grain growth law to $L^m = k(t - t_0)$. Now we combine grain growth law, Eq. 14 and Eq. 15 to obtain expression for the time-dependent interdiffusion coefficient:

$$D(t) = D_{GB} \left[\frac{k}{(q\delta)^m} (t - t_0) \right]^{-1/m} \quad (17a)$$

The meaning of t_0 needs additional specification. Grains in different regions of the product layer begin to grow not at the same time. A grain within PL starts to grow not when the experiment begins, but when the grain nucleates at the reactive boundary, that is, at the passage time, $t^*(x)$, of the reactive boundary through the coordinate x . Eq. 17a can now be rewritten in terms of passage time, with the interdiffusion coefficient dependent on both time and coordinate:

$$D(x, t) = \frac{q\delta D_{GB}}{k^{1/m}} (t - t^*(x))^{-1/m} \quad (17b)$$

We expect that the movement of the reactive boundary is according to the power law $\ell(t) = \lambda t^{1/n}$. Assuming this to be true, we can express the passage time as $t^*(x) = (x/\lambda)^n$, and the diffusion equation Eq. 10 becomes:

$$\frac{\partial C}{\partial t} = \frac{\partial C}{\partial x} \frac{q\delta D_{GB}}{k^{1/m}} \frac{n}{m} \frac{1}{x} \left(\frac{x}{\lambda}\right)^n \left(t - \left(\frac{x}{\lambda}\right)^n\right)^{-\frac{1+m}{m}} + \frac{\partial^2 C}{\partial x^2} \frac{q\delta D_{GB}}{k^{1/m}} \left(t - \left(\frac{x}{\lambda}\right)^n\right)^{-1/m} \quad (18)$$

We search for a self-similar solution of Eq. 18, a solution that can be expressed as a function of a single variable, given by the similarity transformation:

$$z = \frac{x}{\ell(t)} = \frac{x}{\lambda t^{1/n}}$$

This solution exists, if the partial differential equation Eq. 18 transforms to an ordinary differential equation by the similarity transformation. Details of this transformation are given in Appendix A.3. The final result is that a condition on exponents of power-law kinetics (n) and grain growth (m) is imposed:

$$\frac{1}{m} + \frac{2}{n} = 1 \quad (19)$$

This equation gives a convenient means of verification of the proposed model, as both exponents are easy to measure experimentally. Let us also examine the limiting cases of Eq. 19:

- if $m = 2$, then $n = 4$. The value $m = 2$ is the smallest experimentally observed of grain growth exponent, and it is predicted by the grain-growth models and numerical simulations [47, 48, 49, 50, 51, 52, 53]. At the same time, $n = 4$ is the largest growth exponent observed experimentally.
- if $m \rightarrow \infty$, then $n \rightarrow 2$. It means that if no grain growth occurs, Eq. 19 reduces the kinetics to a diffusion control regime with constant interdiffusion coefficient ($\ell \propto \sqrt{t}$), as should be expected.

Eq. 19 connects exponents n and m and shows competition between processes of mass transport and grain boundary movement. If grain growth is slow, than interdiffusion coefficient is almost constant and kinetics of a reaction is parabolic. If grain growth is fast, the grain boundaries (routes of rapid diffusion) move and disappear faster, so the overall reaction kinetics is slower.

Having made the similarity transformation, we can obtain the analytical solution to Eqs. 10–11:

$$\left\{ \begin{array}{l} \ell(t) = \gamma \sqrt{\frac{q\delta D_{GB}}{k^{1/m}}} t^{1/n} \\ C(x, t) = C_{max} - (C_{max} - C_{eq}) \frac{\int_0^{x/\lambda t^{1/n}} (1 - y^n)^{1-2/n} \exp\left[-\frac{\gamma^2}{2n} y^2 F\left(\frac{2-n}{n}, \frac{2}{n}; \frac{2+n}{n}; y^n\right)\right] dy}{\int_0^1 (1 - y^n)^{1-2/n} \exp\left[-\frac{\gamma^2}{2n} y^2 F\left(\frac{2-n}{n}, \frac{2}{n}; \frac{2+n}{n}; y^n\right)\right] dy} \\ n(C_{max} - C_{eq})\tilde{V}_A = \gamma^2 \exp\left[-\frac{\gamma^2}{2n} F\left(\frac{2-n}{n}, \frac{2}{n}; \frac{2+n}{n}; 1\right)\right] \\ \quad \times \int_0^1 (1 - y^n)^{1-2/n} \exp\left[-\frac{\gamma^2}{2n} y^2 F\left(\frac{2-n}{n}, \frac{2}{n}; \frac{2+n}{n}; y^n\right)\right] dy \end{array} \right. \quad (20)$$

$$\quad \quad \quad (21)$$

$$\quad \quad \quad (22)$$

where $F\left(\frac{2-n}{n}, \frac{2}{n}; \frac{2+n}{n}; y^n\right)$ is a Gauss hypergeometric series [54], given by:

$$F\left(\frac{2-n}{n}, \frac{2}{n}; \frac{2+n}{n}; y^n\right) = \frac{\Gamma\left(\frac{2+n}{n}\right)}{\Gamma\left(\frac{2-n}{n}\right) \cdot \Gamma\left(\frac{2}{n}\right)} \sum_{j=0}^{\infty} \frac{\Gamma\left(\frac{2-n}{n} + j\right) \cdot \Gamma\left(\frac{2}{n} + j\right) y^{j \cdot n}}{\Gamma\left(\frac{2+n}{n} + j\right) j!}$$

General structure of the solution is the same as in ordinary diffusion case (Eqs. 7–9), although details are more complicated. Eq. 20 is equation for a width of PL as a function of time; Eq. 21 is equation for concentration within PL as a function of time and coordinate. Eq. 22 determines the numerical factor γ that appears in Eqs. 20 and 21.

For the visual comparison, three profiles (one of ordinary diffusion case and two of diffusion accompanied with grain growth) are shown in Fig. 2. The profiles are constructed for the same width of product layer. One can see how slightly ordinary diffusion profile differs from a straight line (red dashed line),

and how profiles in cases of nonparabolic growth are qualitatively different from it. The latter two are also almost linear within majority of the product layer bulk, but the profiles bend so that the slope becomes vanishingly small near the moving boundary. This feature arises from the grains becoming ever finer near the boundary, and if such profile is observed it should be regarded as another evidence of grain growth.

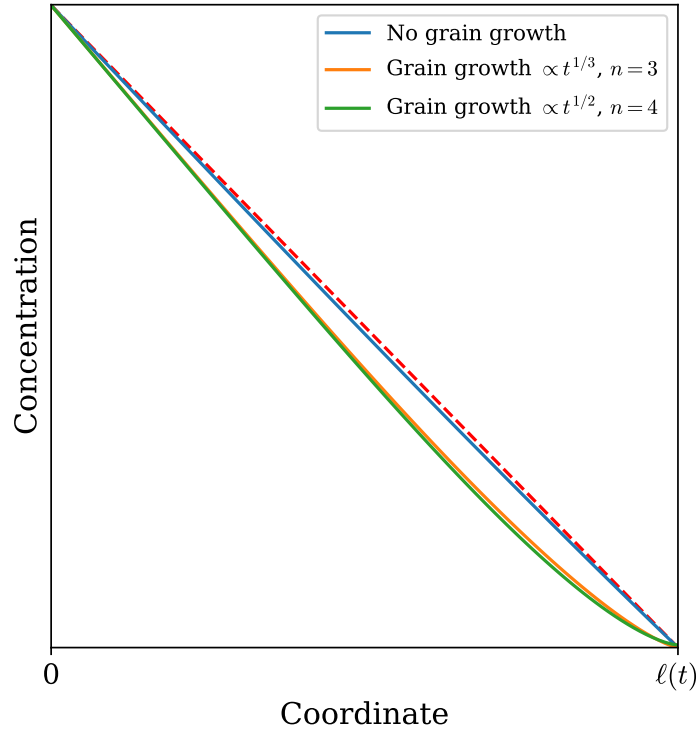


Figure 2: General shape of concentration profiles for different kinetic of product layer growth. Straight line (red dashed) is added as a visual aid.

3. Experimental

Iridium was cut from as-received plate (99.97% purity, GOST 55084-2012, Russia) to size $5 \times 5 \times 0.1$ mm for use in reaction couples. ZrC was preliminary sintered into pellets sized $\varnothing 12 \times 3$ mm from the powder (99.8% purity, $D_{50} = 2$ μm , technical specifications TU 6-09-408-75) by hot pressing at 1900°C under 20 MPa for 30 min. Pellets were polished from one face using a set of diamond suspension (Aquapol-P, Kemet Internation Limited, UK) with particle sizes 9–1 μm . The density of the pellets was 6.512 ± 0.003 g cm⁻³ (measured with Upyc 1200e V5.07), 97% of the theoretical; the lattice parameter was

4.693 Å (refined by Rietveld method using Topas 4.2; XRD data collected on D8 Advance powder diffractometer, Bruker AXS, USA), corresponding to a stoichiometric composition.

Reaction couples were assembled with iridium plate on top of ZrC pellet, heated in UGP Laboratory hot press (IA&E SB RAS, Russia) to a given temperature (1500, 1550 or 1600°C) and held at that temperature for a holding time ranging from 2 to 16 h; a pressure of 5 MPa was applied to the couple to ensure better contact. After annealing, reaction couples were cross-sectioned, packed with an epoxy, and polished with diamond suspension. Morphology was characterized by scanning electron microscopy (SEM) using TM-1000 (Hitachi Ltd, Japan) and MIRA 3 LMU (TESCAN, Czech Republic). Measurements of product layer thickness, carbon particles average area and average grain size were performed on acquired microphotographs using ImageJ [55]. Elemental composition was measured by wavelength-dispersive spectroscopy (WDS) using JXA-8230 electron probe microanalyzer (Jeol Ltd, Japan) at an accelerating voltage of 20 kV; PET (Zr) and LiF (Ir) were used as analyzer crystals, pure iridium (Ir) and zirconium carbide (ZrC) were used as standards to calculate concentrations [14]. Thus were obtained concentration profiles along reaction couples and elemental compositions in vicinity of boundaries Ir/ZrIr₃ and ZrIr₃/ZrC (probes taken in 5 μm from the boundary). The structure of the carbon formed within product layer was characterized by Raman spectroscopy using a microscope LabRam HR Evolution (Horiba, Japan).

4. Results and Discussion

4.1. Morphology and elemental composition

All samples have similar features of the morphology of the product layer (PL). Fig. 3 shows an SEM image of a cross-section of the reaction couple annealed for 8 hours at 1600°C. PL consists of a continuous matrix of ZrIr₃ with small carbon inclusions. The cross-section of PL has a compact polished surface with no voids (SE-SEM images given in Supplement 1), as was expected from that the volume of products (per 1 mol of ZrIr₃) exceeds by 4% the volume of reactants. Carbon inclusions are present throughout the PL, with only a thin region near the Ir/ZrIr₃ interface appearing carbon-free.

Actual presence and structure of carbon was confirmed by Raman spectroscopy. The spectra from black spots throughout the PL always showed the presence of peaks at *ca.* 1330, 1580, and 2660 cm⁻¹ corresponding to D, G, and 2D graphite bands (see Supplement 2). To check the possibility of recrystallization of carbon within the PL, the area of carbon particles was measured along PL from the Ir/ZrIr₃ to ZrIr₃/ZrC interface. Cross-sectional areas of carbon particles are distributed exponentially, with the number of particles decaying with an increase in size (Fig. 4a). Such distribution is probably caused by the process of formation of carbon particles on the reactive boundary, with small particles having a greater probability of formation than the larger ones. Once formed, the carbon particle would not change its size, as can be inferred from Fig. 4b, showing mean and median cross-section areas of carbon particles.

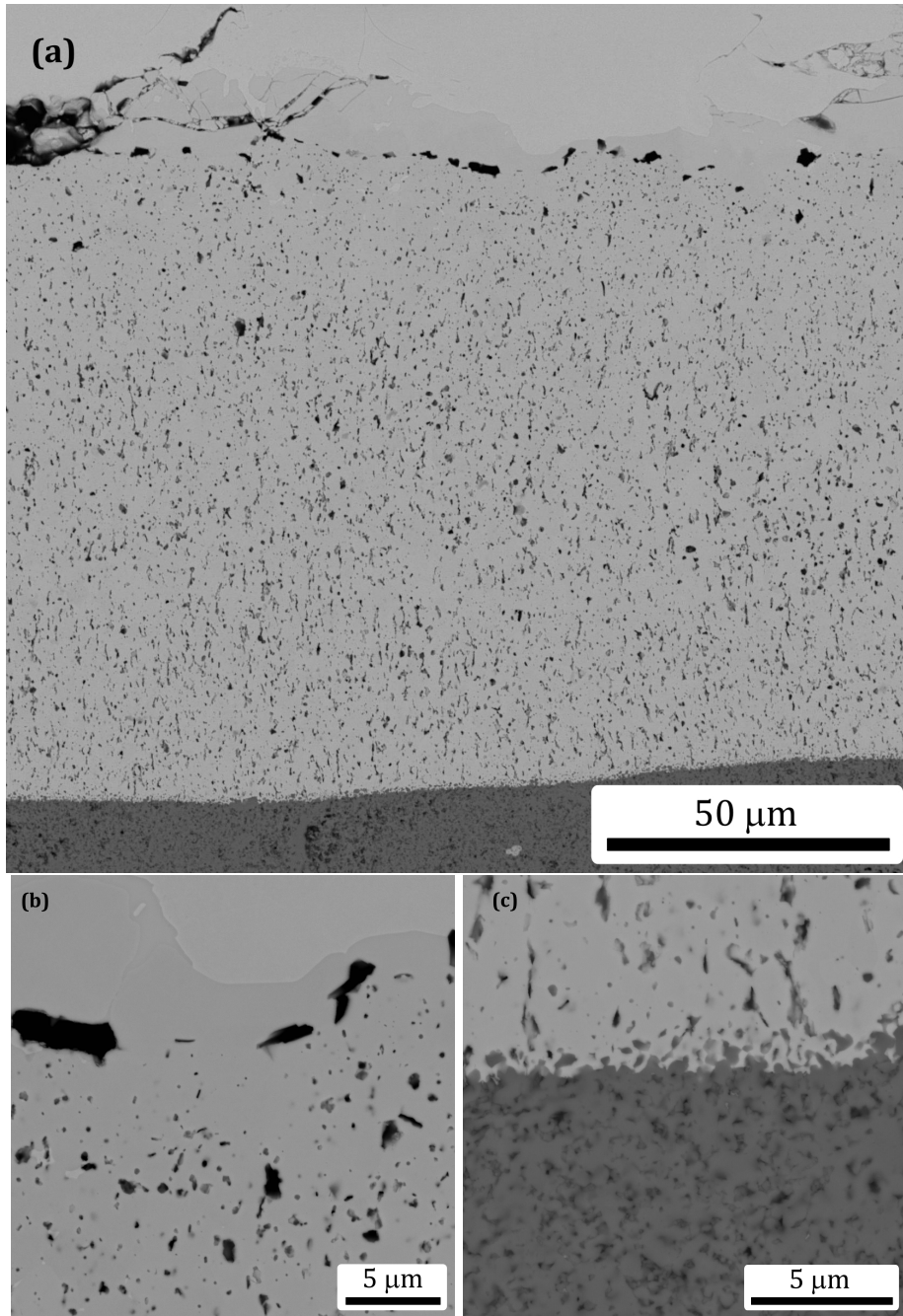


Figure 3: Morphology of a reaction couple; sample shown is heat-treated at 1600°C for 8 h. *a* — general view with all layers shown. *b* — image of the Ir/ZrIr₃ interface. *c* — image of the ZrIr₃/ZrC interface.

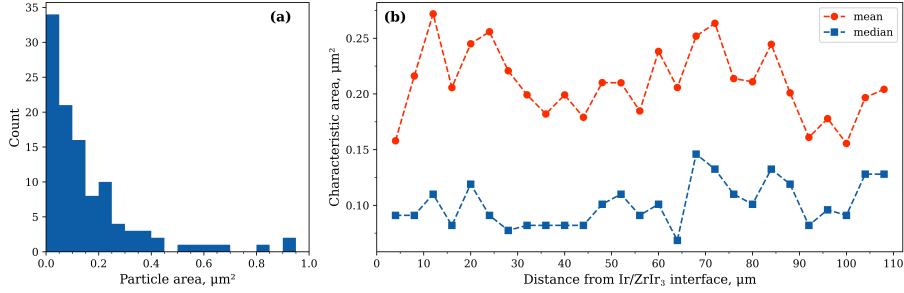


Figure 4: Characterization of carbon within the product layer: *a* — size distribution of carbon particles; *b* — mean and median areas of carbon particles.

Thus, carbon can be regarded as an inert indicator of the reaction at the ZrIr_3/ZrC interface. As noted earlier, the carbon is observed throughout the *PL*, which means the reaction proceeds via reaction with at the ZrIr_3/ZrC interface, while Ir/ZrIr_3 boundary acts as only a source of iridium for the intermetallic phase.

The intermetallic ZrIr_3 phase adopts L_{12} structure type and can form a range of substitutional solid solutions [56], both sub- and over-stoichiometric by iridium. Fig. 5 shows a concentration profile in a region of a reaction couple heat-treated for 8 hours at 1600°C ; other samples show similar features. One can see, that indeed the *PL* contains only one intermetallic compound — ZrIr_3 . This phase is overstoichiometric by Ir, in accordance with previous investigations with powder samples [14, 57]. Composition near the boundary Ir/ZrIr_3 is close to the upper limit of the homogeneity range of $\text{ZrIr}_{3\pm x}$, while the composition near the boundary ZrIr_3/ZrC does not reach values of Ir atomic fraction less than 75%. The seeming absence of the substoichiometric ZrIr_3 suggests that the equilibrium composition of ZrIr_3 in contact with ZrC lies close to 75 mol.%.

4.2. Kinetics of the product layer growth

The plot of the mean thickness of the *PL* versus time is shown in Fig. 6, with error bars showing the standard deviation of the thickness of the *PL*. One can see that the thickening behavior gradually changes with an increase in temperature from 1500 to 1600°C .

First, we consider samples treated at 1500 and 1550°C because they show similar growth kinetics (Fig. 6a, b). Fitting experimental points with existing models showed that the kinetics at these temperatures is best described by Eq. 5, so the reaction at the ZrIr_3/ZrC interface controls the growth of the *PL*.

Fitting the *PL* thickness plots by Eq. 5 gives the following values of the interdiffusion coefficient and reaction rate coefficient: $D = (1.0 \pm 0.2) \cdot 10^{-12} \text{ m}^2/\text{s}$ and $k = (2.9 \pm 0.7) \cdot 10^{-8} \text{ m/s}$ (at 1500°C); $D = (4.0 \pm 1.5) \cdot 10^{-13} \text{ m}^2/\text{s}$ and $k = (5 \pm 8) \cdot 10^{-8} \text{ m/s}$ (at 1550°C). The points at 1500°C are satisfactorily approximated, while the points at 1550°C are approximated poorly, as can be seen from Fig. 6 and large uncertainties in values of D and k . Thus, at 1500°C ,

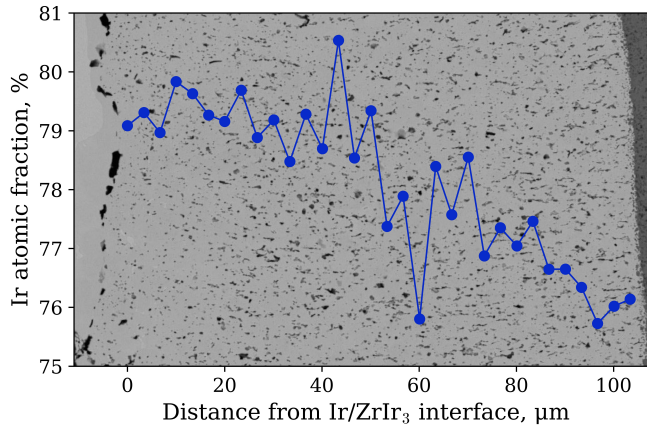


Figure 5: Concentration profile of iridium across the $ZrIr_3$ phase.

kinetics is controlled by the interface reaction, while at 1550°C , the reaction is in a transition regime that is not described well by any model considered in this work.

It is worth noting that the values of the interdiffusion coefficient indicate that diffusion of Ir atoms occurs along grain boundaries. It was shown earlier [58, 59, 60] that the bulk interdiffusion coefficient in L_{12} alloys is by 1–2 orders of magnitude less than the self-diffusion coefficient in a parent metal at the same reduced temperature (T/T_m). At 1616°C (corresponding to reduced temperature $T/T_m = 0.694$ of $ZrIr_3$ at 1500°C) and 1669°C (corresponding to $T/T_m = 0.714$ of $ZrIr_3$ at 1550°C) self-diffusion coefficient of iridium equals $2.64 \cdot 10^{-17}$ and $5.67 \cdot 10^{-17}$ m^2/s accordingly [56, 61]. The interdiffusion coefficients obtained in this work are five orders of magnitude greater than the self-diffusion coefficient of pure iridium, not less than it. That is characteristic of the grain-boundary diffusion, which typically exceeds bulk diffusion by 4–6 orders of magnitude [44].

A similar feature can be noticed in the earlier work of Kwon [15]. This work investigated a reaction between hafnium carbide and iridium at temperatures $1900\text{--}2200^\circ\text{C}$. Kwon found that a product layer ($\text{HfIr}_3 + \text{C}$) grew parabolically and calculated the tracer diffusion coefficient of Ir in HfIr_3 (which contributes the most to the interdiffusion coefficient) from the kinetic data. For instance, it was found that $D_{\text{Ir}}^* = 2.74 \cdot 10^{-14}$ at 2000°C , while the self-diffusion coefficient in elemental Ir at 1981°C (same $T/T_m = 0.828$) is $2.44 \cdot 10^{-15}$. Again, the diffusion in the intermetallic compound appears to be faster than bulk diffusion in pure metal, indicating the grain-boundary character of diffusion. Such behavior might likely be typical for such systems, where the products (intermetallic compound and carbon) form one layer. However, the degree of grain-boundary influence should depend on a particular system.

Secondly, we consider samples annealed at 1600°C . The kinetics of the prod-

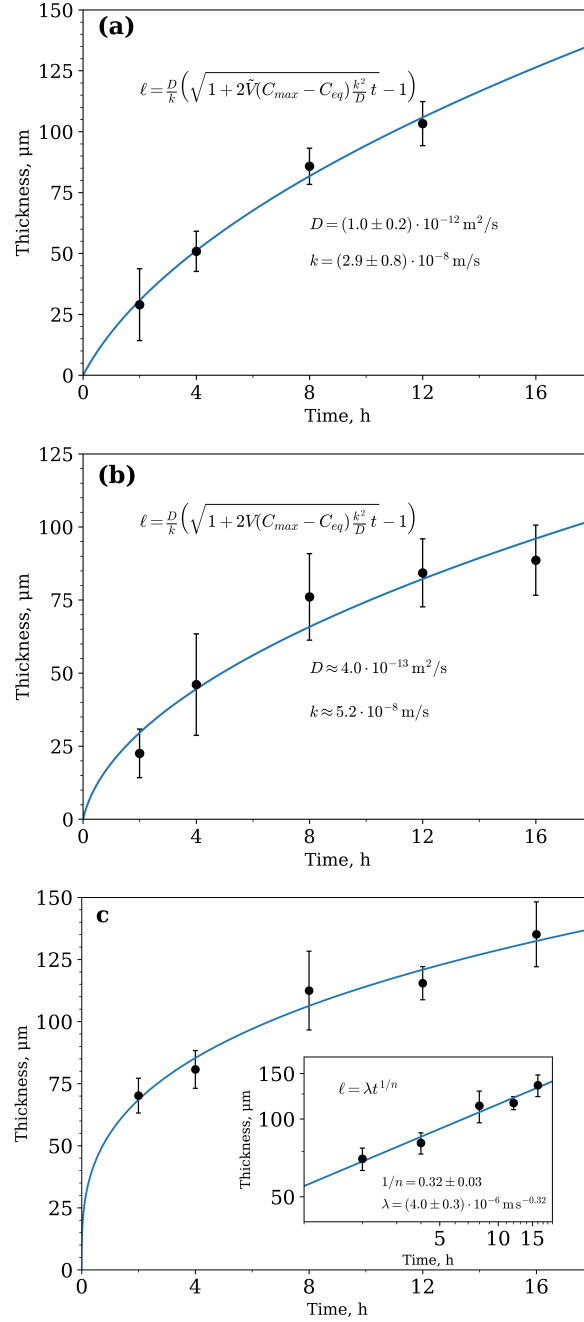


Figure 6: Thickness of the $\text{ZrIr}_3\text{-C}$ layer versus time at three different temperatures: *a* — 1500°C; *b* — 1550°C; *c* — 1600°C.

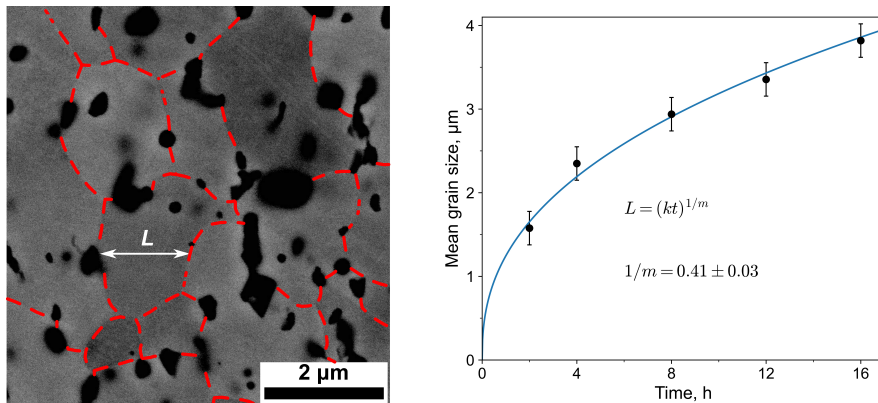


Figure 7: Average grain size in the vicinity of Ir/ZrIr₃ boundary: *a* — delineation of grain boundaries and measurement of cross-sectional length; *b* — plot of average grain size vs. time.

uct layer growth at 1600°C differs from kinetics at 1500 and 1550°C (Fig. 6c) and is described by the power law. Fitting experimental points with Eq. 20 gives values of exponent $n = 0.32 \pm 0.03$ and growth constant $\lambda = (4.0 \pm 0.3) \cdot 10^{-6} \text{ m/s}^{0.32}$.

In Section 2.2, we have argued that non-parabolic growth should be the consequence of grain growth in the *PL*, where diffusion occurs. In the case of the reaction Ir+ZrC, the grain growth should be observable in the ZrIr₃ phase. We have measured the average grain size of ZrIr₃ to support this hypothesis. Because the *PL* grows during the experiment, it is crucial to find a region where the grain size can be correlated unambiguously with the time. That is why the measurements were taken in the vicinity of the Ir/ZrIr₃ interface. This region forms in the initial stages of the reaction and the time of its evolution only slightly differs from the time of the experiment. To find the average size, we used highly contrasted SEM images, then delineated the grain boundaries, measured cross-sectional lengths of grains (Fig. 7), and took the mean value. As the plot in Fig. 7b shows, grain growth obeys the power law Eq. 16 with initial grain size set to zero, following the approximation adopted in Section 2.2. The growth exponent was found to be $m = 0.41 \pm 0.03$. Furthermore, if the model from 2.2 is correct, than the Eq. 19 should hold. Indeed:

$$\frac{1}{m} + \frac{2}{n} = (0.41 \pm 0.03) + 2 \cdot (0.32 \pm 0.03) = 1.05 \pm 0.07$$

the left-hand sum in Eq. 19 calculated from the experimentally measured values of n and m differs from the theoretical value within the uncertainty.

The kinetics of the reaction $\text{ZrC} + 3\text{Ir} \rightarrow \text{ZrIr}_3 + \text{C}$ at studied temperatures can be summarized as follows. The interaction proceeds via reaction at the interface ZrIr₃/ZrC, with iridium atoms diffusing through the *PL* from the Ir/ZrIr₃ boundary. The local equilibrium is reached at the latter boundary, and the products do not form here. At $T < 1500^\circ\text{C}$, and supposedly lower tempera-

tures too, fine grains of ZrIr_3 form. Boundaries of these fine grains are paths of rapid diffusion, so that the overall kinetics is controlled by the reaction at the interface ZrIr_3/ZrC . As temperature rises, the grains start to grow, decreasing the number of grain boundaries and slowing down the diffusion. At 1550°C diffusion is still fast enough, so the kinetics can be regarded as interfacial reaction controlled, but the effect of slowdown becomes noticeable. At 1600°C , the transition to the diffusion-controlled regime occurs, and because the grain growth of ZrIr_3 occurs as well, the PL kinetics obeys the power law with the PL thickness proportional to $t^{0.32}$.

Interestingly, grain growth starts after the mobility of atoms has become noticeably high. Grain growth is commonly associated with the mobility of atoms, but in this case, these phenomena are distinct. It seems plausible that carbon inclusions play some role in it. Carbon inclusions, although not involved in the mass transport themselves, interact with grain boundaries and act as pinning particles [53], slowing down the movement of grain boundaries. Moreover, the grain-growth exponent $m = 1/0.41 \approx 2.4$ is greater than "ideal" $m = 2$, which is highly suggestive of the presence of the pinning effect [62].

We think it would be profitable to study further the effects of grain growth on reaction kinetics in order to fully understand solid-state reactions similar to the one discussed in this work. Here, it turned out that assumptions made in developing the theoretical model were accurate enough to describe experimental data, but one cannot expect it always to be true. It is worth exploring how accounting for non-zero initial grain size, bulk diffusion, and even time-dependent grain growth exponent (which could be observable in some cases [51, 63]) would change the kinetics of a solid-state reaction.

5. Conclusion

In this work, we have studied the solid state reaction between iridium and zirconium carbide at temperatures $1500\text{--}1600^\circ\text{C}$. During the reaction, a product layer consisting of ZrIr_3 and graphite-like carbon forms. Growth of the product layer occurs via the reaction at the ZrIr_3/ZrC interface, while Ir atoms diffuse from the Ir/ZrIr_3 interface through the product layer towards the reaction zone. The carbon acts as an inert secondary phase that forms at the reactive boundary and does not participate in mass transport afterward.

At 1500 and 1550°C , the interaction is in the regime of interfacial reaction control, while at 1600°C , the kinetics is non-parabolic and cannot be properly described as limited by the interfacial reaction or diffusion. This work presents a theoretical treatment of the model of such non-parabolic kinetics. This model accounts for grain growth and its effect on the explicit time dependence of the interdiffusion coefficient. We have obtained full solution for diffusion equation in a growing layer with time-dependent diffusion coefficient and derived the equation that relates grain-growth exponent and the power-law exponent of non-parabolic kinetics. We have shown that the experimental values of these exponents confirm that equation.

Grain boundaries play a significant role in the studied reaction regardless of the kinetics regime. At lower temperatures, boundaries of fine grains of ZrIr_3 provide a path of fast diffusion for iridium atoms, which manifests in the large value of interdiffusion coefficient.

Analysis of the reaction $\text{ZrC} + 3\text{Ir} \longrightarrow \text{ZrIr}_3 + \text{C}$ could be useful beyond the description of the specific system. It provides insight into the behavior of similar systems and what one could expect of them. The role of carbon is essential in such reactions. Although it is an inert secondary phase, it pins grain boundaries of the intermetallic compound, thus slowing down grain growth and ultimately leading to a qualitatively different kinetic regime. Moreover, the theoretical framework presented here will help to understand and further improve our knowledge of interconnection between microstructure and solid-state processes.

Acknowledgements

This study was supported by the Russian Science Foundation (project no. 23-19-00212).

Appendix A. Derivations of results in Theory section

Appendix A.1. Interface reaction control

For the regime of kinetics when the reaction rate is controlled by the interface reaction, the set of the equations 1–4 becomes:

$$\frac{\partial^2 C}{\partial x^2} = 0, \quad 0 \leq x \leq \ell(t) \quad (\text{A.1})$$

$$C(0, t) = C_{max} \quad (\text{A.2})$$

$$\frac{1}{\tilde{V}_A} \frac{d\ell}{dt} = k \cdot (C(\ell) - C_{eq}) = -D \left(\frac{\partial C}{\partial x} \right) \Big|_{x=\ell} \quad (\text{A.3})$$

$$\ell(0) = 0 \quad (\text{A.4})$$

As $\frac{\partial^2 C}{\partial x^2} = 0$, the first derivative of concentration with respect to coordinate is uniform throughout the IL , hence

$$\left(\frac{\partial C}{\partial x} \right) \Big|_{x=\ell} = -\frac{C_{max} - C(\ell)}{\ell}$$

Next, we use the equality between diffusive flux and flux due to interface reaction in (A.3) and

$$k(C(\ell) - C_{eq}) = \frac{D}{\ell}(C_{max} - C(\ell)) \quad \Rightarrow \quad C(\ell) = \frac{kC_{eq} + D/\ell \cdot C_{max}}{k + D/\ell} \quad (\text{A.5})$$

Subsequent substitution into the condition on boundary motion in (A.3) gives:

$$\frac{1}{\tilde{V}_A} \frac{d\ell}{dt} = k \cdot \left(\frac{kC_{eq} + D/\ell \cdot C_{max}}{k + D/\ell} - C_{eq} \right) = \frac{kD/\ell}{k + D/\ell} (C_{max} - C_{eq}) \quad (\text{A.6})$$

The equation A.6 can then be solved by separation of variables, application of initial condition (A.4) and taking the positive branch of the solution:

$$\ell(t) = \frac{D}{k} \left(\sqrt{1 + 2(C_{max} - C_{eq})\tilde{V}_A \frac{k^2}{D} t} - 1 \right) \quad (\text{A.7})$$

Solution for concentration is obtained using the fact, that $C(x)$ is linear:

$$C(x) = C_{max} - \frac{C_{max} - C(\ell)}{\ell} x \quad (\text{A.8})$$

Substituting Eqs. A.5 and A.7 into Eq. A.8, we get the following expression for $C(x, t)$:

$$C(x, t) = C_{max} - \frac{(C_{max} - C_{eq})x}{\sqrt{1 + 2(C_{max} - C_{eq})\tilde{V}_A \frac{k^2}{D} t}} \quad (\text{A.9})$$

Appendix A.2. Diffusion control

In the diffusion controlled regime the set of the equations 1–4 becomes:

$$\frac{\partial C}{\partial t} = D \frac{\partial^2 C}{\partial x^2}, \quad 0 \leq x \leq \ell(t) \quad (\text{A.10})$$

$$C(0, t) = C_{max}, \quad C(\ell, t) = C_{eq} \quad (\text{A.11})$$

$$\frac{1}{\tilde{V}_A} \frac{d\ell}{dt} = -D \left(\frac{\partial C}{\partial x} \right) \Big|_{x=\ell} \quad (\text{A.12})$$

$$\ell(0) = 0 \quad (\text{A.13})$$

This system of equations is solved via a similarity transformation:

$$z = \frac{x}{\lambda t^{1/2}} \quad (\text{A.14})$$

with λ defined such that $\ell(t) = \lambda t^{1/2}$. Then we transform partial derivatives $\partial C/\partial t$ and $\partial^2 C/\partial x^2$ into ordinary derivatives dC/dz and d^2C/dz^2 :

$$\begin{aligned} \frac{\partial C}{\partial t} &= -\frac{z}{2t} \frac{dC}{dz} \\ \frac{\partial^2 C}{\partial x^2} &= \frac{z^2}{x^2} \frac{d^2 C}{dz^2} = \frac{1}{\lambda^2 t} \frac{d^2 C}{dz^2} \end{aligned}$$

Then Eq. A.10 transforms into:

$$-\frac{\lambda^2 z}{2D} \frac{dC}{dz} = \frac{d^2 C}{dz^2} \quad (\text{A.15})$$

Integration of this equation with boundary conditions (Eq. A.11) leads to the following solution:

$$C(x, t) = C_{max} - \frac{C_{max} - C_{eq}}{\operatorname{erf}(\lambda/2\sqrt{D})} \operatorname{erf}\left(\frac{x}{2\sqrt{Dt}}\right) \quad (\text{A.16})$$

At this point it is convenient to introduce a dimensionless parameter $\gamma = \lambda/2\sqrt{D}$, so that the boundary moves according to equation:

$$\ell = 2\gamma\sqrt{Dt} \quad (\text{A.17})$$

and Eq. A.14 becomes:

$$C(x, t) = C_{max} - \frac{C_{max} - C_{eq}}{\operatorname{erf}(\gamma)} \operatorname{erf}\left(\frac{x}{2\sqrt{Dt}}\right) \quad (\text{A.18})$$

Parameter γ can be found with the use of Eq. A.12. After taking derivatives $d\ell/dt$ and $\partial C/\partial x$ and substituting it into Eq. A.12 we obtain the following equation on γ , from which it can be determined:

$$\frac{(C_{max} - C_{eq})\tilde{V}_A}{\sqrt{\pi}} = \gamma \operatorname{erf}(\gamma) \exp(\gamma^2) \quad (\text{A.19})$$

Appendix A.3. Grain-growth accompanied kinetics

This appendix is designed to give a more complete treatment of the model discussed in Section 2.2. First, we will derive a more general diffusion equation when the grain growth is present. Then we will show how the two simplifying assumptions lead to the result obtained earlier in Section 2.2. And lastly, we will show, how the solution to the diffusion equation is obtained. The notation is the same as in Section 2.2.

The system of equations is:

$$\frac{\partial C}{\partial t} = \frac{\partial}{\partial x} \left(D(x, t) \frac{\partial C}{\partial x} \right), \quad 0 \leq x \leq \ell(t) \quad (\text{A.20})$$

$$C(0, t) = C_{max}, \quad C(\ell, t) = C_{eq} \quad (\text{A.21})$$

$$\frac{1}{\tilde{V}_A} \frac{d\ell}{dt} = -D \left(\frac{\partial C}{\partial x} \right) \Big|_{x=\ell} \quad (\text{A.22})$$

$$\ell(0) = 0 \quad (\text{A.23})$$

Time dependence of interdiffusion coefficient can be found with the use of the following equations:

$$D = gD_{GB} + (1 - g)D_B \quad (\text{A.24})$$

$$g = \frac{q\delta}{L} \quad (\text{A.25})$$

$$L^m - L_0^m = k(t - t_0) \quad (\text{A.26})$$

Combining Eqs. A.25 and A.26 and solving for $g(t)$, we obtain:

$$g(t) = \left[g_0^{-m} + \frac{k}{(q\delta)^m} (t - t_0) \right]^{-1/m} \quad (\text{A.27})$$

Inserting it into Eq. A.24 gives the time dependence of the effective interdiffusion coefficient:

$$D(x, t) = D_B + (D_{GB} - D_B) \left[g_0^{-m} + \frac{k}{(q\delta)^m} (t - t^*(x)) \right]^{-1/m} \quad (\text{A.28})$$

where $t^*(x)$ is the time when the moving boundary passes through the coordinate x (passage time); in our case this passage time and time t_0 (start of grain growth) coincide.

The next step is to use the expression of the time-dependent interdiffusion coefficient to find the explicit diffusion equation. To do that, we rewrite Eq. A.20 as:

$$\frac{\partial C}{\partial t} = \frac{\partial D}{\partial x} \frac{\partial C}{\partial x} + D \frac{\partial^2 C}{\partial x^2} \quad (\text{A.29})$$

Then, we express the derivative $\frac{\partial D(x,t)}{\partial x}$:

$$\frac{\partial D(x, t)}{\partial x} = \frac{k(D_{GB} - D_B)}{m(q\delta)^m} \left[g_0^{-m} + \frac{k}{(q\delta)^m} (t - t^*(x)) \right]^{-\frac{1+m}{m}} \frac{dt^*(x)}{dx} \quad (\text{A.30})$$

The diffusion equation (A.29) thus becomes:

$$\begin{aligned} \frac{\partial C}{\partial t} = & \frac{k(D_{GB} - D_B)}{m(q\delta)^m} \left[g_0^{-m} + \frac{k}{(q\delta)^m} (t - t^*(x)) \right]^{-\frac{1+m}{m}} \frac{dt^*(x)}{dx} \frac{\partial C}{\partial x} \\ & + \left[D_B + (D_{GB} - D_B) \left(g_0^{-m} + \frac{k}{(q\delta)^m} (t - t^*(x)) \right)^{-1/m} \right] \frac{\partial^2 C}{\partial x^2} \end{aligned} \quad (\text{A.31})$$

Now we use some assumptions to simplify Eq. A.31. We expect that the movement of the boundary is governed by the power law $\ell(t) = \lambda t^{1/n}$. So we can express the passage time as $t^*(x) = (x/\lambda)^n$. Inserting it into Eqs. A.28 and A.30 we can express the interdiffusion coefficient and its partial derivative $\partial D/\partial x$ as:

$$D(x, t) = D_B + (D_{GB} - D_B) \left[g_0^{-m} + \frac{k}{(q\delta)^m} \left(t - \left(\frac{x}{\lambda} \right)^n \right) \right]^{-1/m} \quad (\text{A.32 a})$$

$$\frac{\partial D(x, t)}{\partial x} = \frac{nk(D_{GB} - D_B)}{m(q\delta)^m x} \left(\frac{x}{\lambda} \right)^n \left[g_0^{-m} + \frac{k}{(q\delta)^m} \left(t - \left(\frac{x}{\lambda} \right)^n \right) \right]^{-\frac{1+m}{m}} \quad (\text{A.32 b})$$

The next assumptions are:

- Grains in the vicinity of the reactive boundary are substantially smaller than grains in the rest of the *PL*: $L_0 \rightarrow 0$. Because $g_0 \propto L_0^{-1}$, we can neglect term g_0^{-m} in square brackets in Eqs. A.32 a and A.32 b.

- Bulk diffusion can be neglected in comparison with the grain-boundary diffusion: $D \approx qD_{GB}$.

Given the aforementioned assumptions, we simplify (A.31) to:

$$\begin{aligned} \frac{\partial C}{\partial t} &= \frac{nkD_{GB}}{m(q\delta)^m x} \left(\frac{x}{\lambda}\right)^n \left[\frac{k}{(q\delta)^m} \left(t - \left(\frac{x}{\lambda}\right)^n\right) \right]^{-\frac{1+m}{m}} \frac{\partial C}{\partial x} \\ &\quad + D_{GB} \left[\frac{k}{(q\delta)^m} \left(t - \left(\frac{x}{\lambda}\right)^n\right) \right]^{-\frac{1}{m}} \frac{\partial^2 C}{\partial x^2} \quad (\text{A.33}) \end{aligned}$$

Eq. A.33 can be solved in a way similar to the solution of Eq. A.10 — introducing a similarity transformation:

$$z = \frac{x}{\lambda t^{1/n}}$$

Partial derivatives, then, are transformed as follows:

$$\begin{aligned} \frac{\partial C}{\partial t} &= \frac{dC}{dz} \frac{\partial z}{\partial t} = -\frac{z}{nt} \frac{dC}{dz} \\ \frac{\partial C}{\partial x} &= \frac{dC}{dz} \frac{\partial z}{\partial x} = \frac{1}{\lambda t^{1/n}} \frac{dC}{dz} \\ \frac{\partial^2 C}{\partial x^2} &= \frac{d^2 C}{dz^2} \left(\frac{\partial z}{\partial x}\right)^2 = \left(\frac{1}{\lambda t^{1/n}}\right)^2 \frac{d^2 C}{dz^2} \end{aligned}$$

We shall leave the time derivative as it is and consider terms in Eq. ?? involving spatial derivatives.

$$\begin{aligned} \frac{\partial D}{\partial x} \frac{\partial C}{\partial x} &= \frac{nkD_{GB}}{m(q\delta)^m x} \left(\frac{x}{\lambda}\right)^n \left[\frac{k}{(q\delta)^m} \left(t - \left(\frac{x}{\lambda}\right)^n\right) \right]^{-\frac{1+m}{m}} \frac{1}{\lambda t^{1/n}} \frac{dC}{dz} \\ &= \frac{dC}{dz} \cdot \frac{1}{\lambda t^{1/n}} \frac{nkD_{GB}}{m(q\delta)^m z \lambda t^{1/n}} z^n t \left[\frac{k}{(q\delta)^m} (t - z^n t) \right]^{-(1+m)/m} \\ &= \frac{dC}{dz} \frac{nq\delta D_{GB}}{m k^{1/m} \lambda^2} z^{n-1} (1 - z^n)^{-(1+m)/m} t^{-\left(\frac{1}{m} + \frac{2}{n}\right)} \\ \\ D \frac{\partial^2 C}{\partial x^2} &= D_{GB} \left[\frac{k}{(q\delta)^m} \left(t - \left(\frac{x}{\lambda}\right)^n\right) \right]^{-\frac{1}{m}} \frac{d^2 C}{dz^2} \\ &= \frac{d^2 C}{dz^2} \cdot D_{GB} \frac{1}{\lambda^2 t^{2/n}} \left[\frac{k}{(q\delta)^m} (t - z^n t) \right]^{-1/m} \\ &= \frac{d^2 C}{dz^2} \frac{q\delta D_{GB}}{k^{1/m} \lambda^2} (1 - z^n)^{-1/m} t^{-\left(\frac{1}{m} + \frac{2}{n}\right)} \end{aligned}$$

Note that $\frac{\partial C}{\partial t}$, $\frac{\partial D}{\partial x} \frac{\partial C}{\partial x}$ and $D \frac{\partial^2 C}{\partial x^2}$ depend only on z and a power of time. For a solution to exist, the powers of time must cancel. It can be achieved with condition:

$$\frac{1}{m} + \frac{2}{n} = 1 \quad (\text{A.34})$$

Thus, Eq. A.34 connects the exponent of grain growth, m , and the exponent of the power law, n .

Now, we solve for $C(x, t)$. After the similarity transformation, Eq. A.31 becomes:

$$\frac{d^2 C}{dz^2} \frac{q\delta D_{GB}}{k^{1/m}\lambda^2} (1-z^n)^{-1/m} + \frac{dC}{dz} \left[\frac{n}{m} \frac{q\delta D_{GB}}{k^{1/m}\lambda^2} z^{n-1} (1-z^n)^{-(1+m)/m} + \frac{z}{n} \right] = 0 \quad (\text{A.35})$$

We introduce a dimensionless constant $\gamma = \lambda k^{1/2m} / \sqrt{q\delta D_{GB}}$ and use Eq. A.34, changing $1/m$ to $(1-2/n)$ and n/m to $(n-2)$:

$$\frac{d^2 C}{dz^2} \frac{1}{\gamma^2} (1-z^n)^{2/n-1} + \frac{dC}{dz} \left[\frac{n-2}{\gamma^2} z^{n-1} (1-z^n)^{2/n-2} + \frac{z}{n} \right] = 0 \quad (\text{A.36})$$

Integration of Eq. A.36 gives the following solution:

$$C(x, t) = A_1 - A_2 \int_0^{x/\lambda t^{1/n}} (1-y^n)^{1-2/n} \exp \left[-\frac{\gamma^2}{2n} y^2 F \left(\frac{2-n}{n}, \frac{2}{n}; \frac{2+n}{n}; y^n \right) \right] dy$$

where A_1 and A_2 are constants of integration, $F(\frac{2-n}{n}, \frac{2}{n}; \frac{2+n}{n}; y^n)$ is a Gauss hypergeometric series.

Condition (Eq. A.21) on the A/PL boundary gives $A_1 = C_{max}$, while condition on the PL/B boundary gives:

$$A_2 = (C_{max} - C_{eq}) / \int_0^1 (1-y^n)^{1-2/n} \exp \left[-\frac{\gamma^2}{2n} y^2 F \left(\frac{2-n}{n}, \frac{2}{n}; \frac{2+n}{n}; y^n \right) \right] dy$$

The value of yet undetermined constant γ can be obtained from the condition on the moving boundary (Eq. A.22). This condition produces a transcendental equation on γ , so it must be sought numerically in every particular case. Thus, a solution for a solid-state reaction, limited by diffusion, with grain-growth of the PL , is given by:

$$\left\{ \begin{array}{l} \ell(t) = \gamma \sqrt{\frac{q\delta D_{GB}}{k^{1/m}}} t^{1/n} \end{array} \right. \quad (\text{A.37})$$

$$\left\{ \begin{array}{l} C(x, t) = C_{max} - (C_{max} - C_{eq}) \frac{\int_0^{x/\lambda t^{1/n}} (1-y^n)^{1-2/n} \exp \left[-\frac{\gamma^2}{2n} y^2 F \left(\frac{2-n}{n}, \frac{2}{n}; \frac{2+n}{n}; y^n \right) \right] dy}{\int_0^1 (1-y^n)^{1-2/n} \exp \left[-\frac{\gamma^2}{2n} y^2 F \left(\frac{2-n}{n}, \frac{2}{n}; \frac{2+n}{n}; y^n \right) \right] dy} \end{array} \right. \quad (\text{A.38})$$

$$\left\{ \begin{array}{l} n(C_{max} - C_{eq}) \tilde{V}_A = \gamma^2 \exp \left[-\frac{\gamma^2}{2n} F \left(\frac{2-n}{n}, \frac{2}{n}; \frac{2+n}{n}; 1 \right) \right] \\ \quad \times \int_0^1 (1-y^n)^{1-2/n} \exp \left[-\frac{\gamma^2}{2n} y^2 F \left(\frac{2-n}{n}, \frac{2}{n}; \frac{2+n}{n}; y^n \right) \right] dy \end{array} \right. \quad (\text{A.39})$$

References

- [1] W.-P. Wu, Z.-F. Chen, Iridium coating: Processes, properties and application. Part I, Johnson Matthey Technology Review 61 (2017) 16–28. doi:10.1595/205651317x693606.

- [2] W.-P. Wu, Z.-F. Chen, Iridium coating: Processes, properties and application. Part II, *Johnson Matthey Technology Review* 61 (2017) 93–110. doi:10.1595/205651317X695064.
- [3] J. Arblaster, The thermodynamic properties of iridium on ITS-90, *Calphad* 19 (1995) 365–372. doi:10.1016/0364-5916(95)00034-C.
- [4] J. M. Criscione, R. A. Mercuri, E. P. Schram, A. W. Smith, H. F. Volk, High temperature protective coatings for graphite — Part II, *Tech. rep.*, Air Force Materials Laboratory (1964).
- [5] K. Mumtaz, J. Echigoya, H. Enoki, T. Hirai, Y. Shindo, Thermal cycling of iridium coatings on isotropic graphite, *J. Mater. Sci.* 30 (1995) 465–472. doi:10.1007/bf00354413.
- [6] W. Wu, Z. Chen, H. Cheng, L. Wang, Y. Zhang, Tungsten and iridium multilayered structure by DGP as ablation-resistance coatings for graphite, *Appl. Surf. Sci.* 257 (2011) 7295–7304. doi:10.1016/j.apsusc.2011.03.108.
- [7] L. Zhu, S. Bai, H. Zhang, Y. Ye, W. Gao, Rhenium used as an inter-layer between carbon-carbon composites and iridium coating: Adhesion and wettability, *Surf. Coat. Technol.* 235 (2013) 68–74. doi:10.1016/j.surfcoat.2013.07.013.
- [8] L. Zhu, S. Bai, H. Zhang, Y. Ye, W. Gao, Double-layer iridium-aluminum intermetallic coating on iridium/rhenium coated graphite prepared by pack cementation, *Surf. Coat. Technol.* 258 (2014) 524–530. doi:10.1016/j.surfcoat.2014.08.044.
- [9] Z. Chen, W. Wu, X. Cong, Oxidation resistance coatings of Ir-Zr and Ir by double glow plasma, *J. Mater. Sci. Technol.* 30 (2014) 268–274. doi:10.1016/j.jmst.2013.06.002.
- [10] L. Zhu, G. Du, S. Bai, H. Zhang, Y. Ye, Y. Ai, Oxidation behavior of a double-layer iridium-aluminum intermetallic coating on iridium at the temperature of 1400°C–2000°C in the air atmosphere, *Corros. Sci.* 123 (2017) 328–338. doi:10.1016/j.corsci.2017.05.010.
- [11] K. Zhang, L. Zhu, S. Bai, Y. Ye, H. Zhang, S. Li, Y. Tang, J. Zhang, G. Wang, Ablation behavior of an Ir-Hf coating: A novel idea for ultra-high temperature coatings in non-equilibrium conditions, *J. Alloy. Compd.* 818 (2020) 152829. doi:10.1016/j.jallcom.2019.152829.
- [12] H. Zhang, L.-A. Zhu, S.-X. Bai, Y.-C. Ye, Ablation-resistant Ir/Re coating on C/C composites at ultra-high temperatures, *Rare Metals* 41 (2022) 199–208. doi:10.1007/s12598-015-0509-2.

- [13] F. Li, L. Zhu, K. Zhang, Z. Wang, Y. Ye, S. Li, Y. Tang, S. Bai, Ir–Zr coating through a pack cementation method for ultra-high temperature applications, *J. Mater. Res. Technol.* 28 (2024) 4428–4436. doi:10.1016/j.jmrt.2024.01.067.
- [14] Y. A. Nikiforov, V. A. Danilovsky, V. V. Lozanov, N. I. Baklanova, High-temperature solid-state reaction between zirconium carbide and iridium: New insights into the phase formation, *J. Am. Ceram. Soc.* (2024). doi:10.1111/jace.19675.
- [15] J.-W. Kwon, Formation and growth of Ir₃Hf layers at Ir/HfC interfaces between 1900°C and 2200°C (1989) 133.
- [16] J. Park, K. Landry, J. Perepezko, Kinetic control of silicon carbide/metal reactions, *Mater. Sci. Eng.: A* 259 (1999) 279–286. doi:10.1016/S0921-5093(98)00899-5.
- [17] K. Bhanumurthy, R. Schmid-Fetzer, Interface reactions between silicon carbide and metals (Ni, Cr, Pd, Zr), *Composites Part A: Appl. Sci. Manuf.* 32 (2001) 569–574. doi:10.1016/S1359-835X(00)00049-X.
- [18] P. Demkowicz, K. Wright, J. Gan, D. Petti, High temperature interface reactions of TiC, TiN, and SiC with palladium and rhodium, *Solid State Ionics* 179 (2008) 2313–2321. doi:10.1016/j.ssi.2008.07.021.
- [19] E. López-Honorato, K. Fu, P. J. Meadows, J. Tan, P. Xiao, Effect of microstructure on the resilience of silicon carbide to palladium attack, *J. Am. Ceram. Soc.* 93 (2010) 4135–4141. doi:10.1111/j.1551-2916.2010.04005.x.
- [20] M. Gentile, P. Xiao, T. Abram, Palladium interaction with silicon carbide, *J. Nucl. Mater.* 462 (2015) 100–107. doi:10.1016/j.jnucmat.2015.03.013.
- [21] M. A. Golosov, A. V. Utkin, V. V. Lozanov, A. T. Titov, N. I. Baklanova, Microstructural patterning of the reaction zone formed by solid-state interaction between iridium and SiC ceramics, *Materialia* 27 (3 2023). doi:10.1016/j.mtla.2022.101647.
- [22] L. Harrison, The theory of solid phase kinetics, in: C. Bamford, C. Tiper (Eds.), *The Theory of Kinetics*, Vol. 2 of *Comprehensive Chemical Kinetics*, Elsevier, 1969, pp. 377–462. doi:10.1016/B978-0-444-40674-3.50011-0.
- [23] K. Suzuki, S. Kano, M. Kajihara, N. Kurokawa, K. Sakamoto, Reactive diffusion between Ag and Sn at solid state temperatures, *Materials Transactions* 46 (2005) 969–973. doi:10.2320/matertrans.46.969.

- [24] L. Xu, Y. Y. Cui, Y. L. Hao, R. Yang, Growth of intermetallic layer in multi-laminated Ti/Al diffusion couples, *Mater. Sci. Eng.: A* 435-436 (2006) 638–647. doi:10.1016/j.msea.2006.07.077.
- [25] Z. Ren, X. Hu, X. Xue, K. Chou, Solid state reaction studies in Fe_3O_4 - TiO_2 system by diffusion couple method, *J. Alloy. Compd.* 580 (2013) 182–186. doi:10.1016/j.jallcom.2013.05.114.
- [26] A. Gueydan, B. Domengès, E. Hug, Study of the intermetallic growth in copper-clad aluminum wires after thermal aging, *Intermetallics* 50 (2014) 34–42. doi:10.1016/j.intermet.2014.02.007.
- [27] P. T. Vianco, K. L. Erickson, P. L. Hopkins, Solid state intermetallic compound growth between copper and high temperature, tin-rich solders — Part I: Experimental analysis, *J. Electron. Mater.* 23 (1994) 721–727. doi:10.1007/bf02651365.
- [28] S. Bader, W. Gust, H. Hieber, Rapid formation of intermetallic compounds interdiffusion in the Cu-Sn and Ni-Sn systems, *Acta Metallurgica et Materialia* 43 (1995) 329–337. doi:10.1016/0956-7151(95)90289-9.
- [29] M. Mita, M. Kajihara, N. Kurokawa, K. Sakamoto, Growth behavior of Ni_3Sn_4 layer during reactive diffusion between Ni and Sn at solid-state temperatures, *Mater. Sci. Eng.: A* 403 (2005) 269–275. doi:10.1016/j.msea.2005.05.012.
- [30] T. Sakama, M. Kajihara, Influence of Ag on kinetics of solid-state reactive diffusion between Pd and Sn, *Materials Transactions* 50 (2009) 266–274. doi:10.2320/matertrans.mra2008292.
- [31] J. Li, P. Agyakwa, C. Johnson, Kinetics of Ag_3Sn growth in Ag-Sn-Ag system during transient liquid phase soldering process, *Acta Materialia* 58 (2010) 3429–3443. doi:10.1016/j.actamat.2010.02.018.
- [32] M. Mirjalili, M. Soltanieh, K. Matsuura, M. Ohno, On the kinetics of TiAl_3 intermetallic layer formation in the titanium and aluminum diffusion couple, *Intermetallics* 32 (2013) 297–302. doi:10.1016/j.intermet.2012.08.017.
- [33] A. Lis, M. S. Park, R. Arroyave, C. Leinenbach, Early stage growth characteristics of Ag_3Sn intermetallic compounds during solid-solid and solid-liquid reactions in the Ag-Sn interlayer system: Experiments and simulations, *J. Alloy. Compd.* 617 (2014) 763–773. doi:10.1016/j.jallcom.2014.08.082.
- [34] C. Q. Zhang, W. Liu, Abnormal effect of temperature on intermetallic compound layer growth at aluminum-titanium interface: The role of grain boundary diffusion, *Mater. Lett.* 254 (2019) 1–4. doi:10.1016/j.matlet.2019.07.013.

- [35] M. Oh, K. Matsushita, E. Kobayashi, M. Kajihara, The growth kinetics of intermetallic compounds by the fast diffusion path at the interface of Co and molten Zn, *J. Mol. Liq.* 413 (2024) 125966. doi:10.1016/j.molliq.2024.125966.
- [36] P. Murray, G. Carey, Finite element analysis of diffusion with reaction at a moving boundary, *J. Comput. Phys.* 74 (1988) 440–455. doi:10.1016/0021-9991(88)90087-3.
- [37] C. Wagner, The evaluation of data obtained with diffusion couples of binary single-phase and multiphase systems, *Acta Metallurgica* 17 (1969) 99–107. doi:10.1016/0001-6160(69)90131-x.
- [38] P. C. Lichtner, E. H. Oelkers, H. C. Helgeson, Exact and numerical solutions to the moving boundary problem resulting from reversible heterogeneous reactions and aqueous diffusion in a porous medium, *J. Geophys. Res.: Solid Earth* 91 (1986) 7531–7544. doi:10.1029/jb091ib07p07531.
- [39] K. L. Erickson, P. L. Hopkins, P. Vianco, Solid state intermetallic compound growth between copper and high temperature, tin-rich solders — Part II: Modeling, *J. Electron. Mater.* 23 (1994) 729–734. doi:10.1007/bf02651366.
- [40] M. Schaefer, R. A. Fournelle, J. Liang, Theory for intermetallic phase growth between cu and liquid Sn-Pb solder based on grain boundary diffusion control, *J. Electron. Mater.* 27 (1998) 1167–1176. doi:10.1007/s11664-998-0066-7.
- [41] G. Ghosh, Coarsening kinetics of Ni₃Sn₄ scallops during interfacial reaction between liquid eutectic solders and Cu/Ni/Pd metallization, *J. Appl. Phys.* 88 (2000) 6887–6896. doi:10.1063/1.1321791.
- [42] L. Wang, Y. Wang, P. Prangnell, J. Robson, Modeling of intermetallic compounds growth between dissimilar metals, *Metall. Mater. Trans. A: Phys. Metall. Mater. Sci.* 46 (2015) 4106–4114. doi:10.1007/s11661-015-3037-7.
- [43] L. Xu, J. D. Robson, L. Wang, P. B. Prangnell, The influence of grain structure on intermetallic compound layer growth rates in Fe-Al dissimilar welds, *Metall. Mater. Trans. A: Phys. Metall. Mater. Sci.* 49 (2018) 515–526. doi:10.1007/s11661-017-4352-y.
- [44] Y. Mishin, C. Herzig, J. Bernardini, W. Gust, Grain boundary diffusion: Fundamentals to recent developments, *Int. Mater. Rev.* 42 (1997) 155–178. doi:10.1179/imr.1997.42.4.155.
- [45] R. Abbaschian, L. Abbaschian, R. E. Reed-Hill, *Physical Metallurgy Principles*, 4th Edition, Cengage Learning, 2008.

- [46] D. A. Molodov, *Microstructural Design of Advanced Engineering Materials*, 2013. doi:10.1002/9783527652815.
- [47] H. Hu, B. B. Rath, On the time exponent in isothermal grain growth, *Metall. Trans.* 1 (1970) 3181–3184. doi:10.1007/bf03038435.
- [48] N. P. Louat, On the theory of normal grain growth, *Acta Metallurgica* 22 (6) (1974) 721–724. doi:10.1016/0001-6160(74)90081-9.
- [49] M. P. Anderson, G. S. Grest, D. J. Srolovitz, Computer simulation of normal grain growth in three dimensions, *Philos. Mag. B* 59 (3) (1989) 293–329. doi:10.1080/13642818908220181.
- [50] J. Gao, R. G. Thompson, Real time-temperature models for Monte Carlo simulations of normal grain growth, *Acta Materialia* 44 (11) (1996) 4565–4570. doi:10.1016/1359-6454(96)00079-1.
- [51] G. Liu, H. Yu, X. Song, X. Qin, A new model of three-dimensional grain growth: Theory and computer simulation of topology-dependency of individual grain growth rate, *Mater. Des.* 22 (1) (2001) 33–38. doi:10.1016/s0261-3069(00)00040-6.
- [52] Q. Yu, S. K. Esche, Three-dimensional grain growth modeling with a Monte Carlo algorithm, *Mater. Lett.* 57 (30) (2003) 4622–4626. doi:10.1016/s0167-577x(03)00372-0.
- [53] F. Najafkhani, S. Kheiri, B. Pourbahari, H. Mirzadeh, Recent advances in the kinetics of normal/abnormal grain growth: a review, *Arch. Civ. Mech. Eng.* 21 (2021) 29. doi:10.1007/s43452-021-00185-8.
- [54] F. Oberhettinger, Hypergeometric functions, in: M. Abramowitz, I. Stegun (Eds.), *Handbook of Mathematical Functions*, 10th Edition, National Bureau of Standards, 1972, Ch. 15, pp. 555–566.
- [55] C. A. Schneider, W. S. Rasband, K. W. Eliceiri, NIH Image to ImageJ: 25 years of image analysis, *Nature Methods* 2012 9:7 9 (2012) 671–675. doi:10.1038/nmeth.2089.
- [56] H. Ran, Z. Du, Thermodynamic assessment of the Ir–Zr system, *J. Alloy. Compd.* 413 (2006) 101–105. doi:10.1016/j.jallcom.2005.06.060.
- [57] L. Brewer, P. Wengert, Thermodynamic stability of certain intermetallic compounds made from transition elements, *Metall. Trans.* (1973) 15–18.
- [58] T. Ikeda, A. Almazouzi, H. Numakura, M. Koiwa, W. Sprengel, H. Nakajima, Single-phase interdiffusion in Ni₃Al, *Acta Materialia* 46 (1998) 5369–5376. doi:10.1016/s1359-6454(98)00209-2.
- [59] H. Numakura, T. Ikeda, H. Nakajima, M. Koiwa, Diffusion in Ni₃Al, Ni₃Ga and Ni₃Ge, *Mater. Sci. Eng.: A* 312 (2001) 109–117. doi:10.1016/s0921-5093(00)01864-5.

- [60] M. Uchida, H. Numakura, Y. Yamabe-Mitarai, E. Bannai, Chemical diffusion in Ir₃Nb, *Scr. Materialia* 52 (2005) 11–15. doi:10.1016/j.scriptamat.2004.09.006.
- [61] H. Mehrer, N. Stolica, N. A. Stolwijk, 2.2.10 Nickel group metals, Vol. 26, Springer-Verlag, 1990, pp. 52–54. doi:10.1007/b37801.
- [62] E. A. Grey, G. T. Higgins, Solute limited grain boundary migration: A rationalisation of grain growth, *Acta Metall.* 21 (1973) 309–321. doi:10.1016/0001-6160(73)90186-7.
- [63] H. S. Kim, H. J. Lee, Y. S. Yu, Y. S. Won, Three-dimensional simulation of intermetallic compound layer growth in a binary alloy system, *Acta Materialia* 57 (2009) 1254–1262. doi:10.1016/j.actamat.2008.11.006.